

# A finite volume method preserving the invariant region property for the quasimonotone reaction-diffusion systems

Huifang Zhou<sup>1,\*</sup>, Yuchen, Sun<sup>1</sup>, Fuchang Huo<sup>1</sup>,

<sup>1</sup> School of Mathematics, Jilin University, Changchun 130012, P.R. China

---

**Abstract.** We present a finite volume method preserving the invariant region property (IRP) for the reaction-diffusion systems with quasimonotone functions, including nondecreasing, decreasing, and mixed quasimonotone systems. The diffusion terms and time derivatives are discretized by a finite volume method satisfying the discrete maximum principle (DMP) and the backward Euler method, respectively. The discretization leads to an implicit and nonlinear scheme, and it is proved to preserve the invariant region property unconditionally. We construct an iterative algorithm and prove the invariant region property at each iteration step. Numerical examples are shown to confirm the accuracy and invariant region property of our scheme.

**AMS subject classifications:** 65M08, 35K59

**Key words:** Reaction-diffusion systems, quasimonotone, nonlinear finite volume scheme, invariant region, distorted meshes.

---

## 1 Introduction

Reaction-diffusion systems are mathematical models that describe the behaviors of a large range of physical, biological, chemical and electrical phenomena [1, 2, 9, 12, 18]. They are utilized to mimic the variations in chemical substance concentrations caused by local reactions and diffusions in the field of chemistry, as well as the spread of infectious diseases and population growth [10] in biology; the neutron diffusion theory and the Ginzburg–Landau equations for modeling superconductivity [4] in physics; and the FitzHugh–Nagumo model for simulating the transmission of electrical impulses in neurology and so on.

It is of great importance for the numerical methods to preserve the IRP. The IRP refers to the property of reaction-diffusion systems that the solution lies in the range of the

---

\*Corresponding author. *Email addresses:* zhouhuifang@jlu.edu.cn (H. Zhou), sunyc21@mails.jlu.edu.cn (Y. Sun), huofc22@mails.jlu.edu.cn (F. Huo)

initial and boundary values, it reflects the physical constraints of the unknown variables. Hence the numerical solution is expected to preserve the IRP as well. Besides, the IRP of numerical schemes has great importance in establishing the prior estimates, existence and stability of the solution [17]. Proposing the IRP-preserving schemes for reaction-diffusion equations is necessary in both physical and mathematical aspects. The finite difference methods [3, 8, 11, 13] have been widely applied to solve the reaction-diffusion equations because of simplicity. [11] employs a fully implicit time-discretization method, and establishes the IRP and stability of the scheme by M-matrix analysis. [13] combines exponential time differencing method and overlapping domain decomposition technique to get a maximum bound principle (MBP) preserving method for the one-component reaction-diffusion equations, where MBP can be viewed as a special type of invariant region. In [3], the nonstandard finite difference method combined with time-accurate and high stable explicit method is constructed to obtain the positivity-preserving scheme for the reaction-diffusion model describing the vegetation evolution in arid environments. In [8], the authors use the  $\theta$ -weighted time-stepping scheme and corresponding iterative approach for a class of semilinear parabolic equations, where the discrete MBP holds under the constraint of time step and mesh size. However, most finite difference methods are restricted to rectangular meshes. In addition, the finite element method with implicit-explicit Euler time-discretization is employed to solve the 3D reaction-diffusion systems in [7], where the IRP is preserved on Delaunay triangular meshes. The nonlinear Galerkin method is used in [14] to solve the system of reaction-diffusion equations, in which the algorithm needs to calculate the orthonormal basis of the space composed of eigenvectors of the diffusion operator. In [19], the finite volume method preserving the IRP is applied to a specific type of reaction-diffusion systems called FitzHugh-Nagumo equation on polygonal meshes. [5] develops the unified framework which covers many numerical schemes to obtain a MBP-preserving method for the semilinear parabolic equations.

The goal of this paper is to propose an IRP-preserving finite volume method for the coupled quasimonotone parabolic systems on distorted meshes. Compared to our previous work that can only handle specific nonlinear reaction terms in [19], i.e.,  $f_1(u, v) = u(1-u)(u-a) - v$ ,  $f_2(u, v) = \rho u - \gamma v$ , this work can handle more general nonlinear reaction terms. We utilize the DMP-preserving finite volume scheme to discretize the spacial derivatives, and employ the fully implicit scheme to discretize the temporal derivatives. For the problem with three basic types of quasimonotone functions, we analyze that the implicit scheme is unconditionally IRP-preserving and exists at least one solution. To solve the nonlinear scheme, we add a specific linear term in the iterative algorithm and prove the IRP of the iterative method. Numerical results demonstrate that our scheme reaches second-order accuracy in spacial direction and preserves the IRP for different problems. We also present the comparison result with the nine-point scheme to demonstrate that it cannot preserve the IRP.

This paper is organized as follows. Section 2 gives the model problem and its corresponding invariant region theory. In Section 3, the fully implicit finite volume scheme

is presented and the IRP is discussed. In Section 4, the iterative approach is introduced and its IRP is analyzed. In Section 5, we give numerical experiments to demonstrate the accuracy and preservation of IRP. Finally, the Section 6 provides a summary of this paper.

## 2 Invariant region theory of the model problem

In this paper, we will investigate the coupled system of two parabolic equations on a bounded space-time domain  $Q_T = \Omega \times (0, T]$  as

$$\partial_t u - \nabla \cdot (\kappa_1 \nabla u) = f_1(u, v), \quad \text{in } Q_T, \quad (2.1)$$

$$\partial_t v - \nabla \cdot (\kappa_2 \nabla v) = f_2(u, v), \quad \text{in } Q_T, \quad (2.2)$$

subject to the initial conditions  $u(\mathbf{x}, 0) = u_0(\mathbf{x})$  and  $v(\mathbf{x}, 0) = v_0(\mathbf{x})$  on  $\Omega$  and Dirichlet boundary conditions  $u(\mathbf{x}, t) = g_1(\mathbf{x}, t)$  and  $v(\mathbf{x}, t) = g_2(\mathbf{x}, t)$  on  $S_T = \partial\Omega \times (0, T]$ . We suppose  $\Omega$  is an open bounded polygonal domain in  $\mathbb{R}^2$ ,  $\partial\Omega \in C^2$ ,  $\kappa_1$  and  $\kappa_2$  are coercive tensor-valued functions,  $f_1$  and  $f_2$  are nonlinear functions of  $u$  and  $v$ .

The notations of standard Sobolev spaces are employed, with  $(\cdot, \cdot)$  representing the  $L^2(Q_T)$  inner-product. Define bilinear forms  $B_1(u, \phi_1) = (-u\partial_t\phi_1 + \kappa_1\nabla u, \nabla\phi_1)$  and  $B_2(v, \phi_2) = (-v\partial_t\phi_2 + \kappa_2\nabla v, \nabla\phi_2)$ . We say a function  $(u, v) \in [W_2^{1,1}(Q_T) \cap L^\infty(Q_T)]^2$  is a weak solution of the problem (2.1)-(2.2) provided that

(i) for any  $(\phi_1, \phi_2) \in [W_2^{1,1}(Q_T)]^2$  and  $(\phi_1(\mathbf{x}, T), \phi_2(\mathbf{x}, T)) = 0$  a.e. in  $\Omega$ , there hold that

$$\begin{aligned} B_1(u, \phi_1) &= (f_1(u, v), \phi_1), \\ B_2(v, \phi_2) &= (f_2(u, v), \phi_2); \end{aligned}$$

(ii)  $u(\mathbf{x}, 0) = u_0(\mathbf{x})$ ,  $v(\mathbf{x}, 0) = v_0(\mathbf{x})$  a.e. in  $\Omega$  in the sense of trace;

(iii)  $u(\mathbf{x}, t) = g_1(\mathbf{x}, t)$ ,  $v(\mathbf{x}, t) = g_2(\mathbf{x}, t)$  a.e. on  $S_T$  in the sense of trace.

**Definition 2.1. (Invariant region property)** A closed subset  $\Sigma = [m_1, M_1] \times [m_2, M_2]$  is called an invariant region of the problem (2.1)-(2.2) if for almost every  $(u_0, v_0)$  and  $(g_1, g_2) \in \Sigma$ , the corresponding solution  $(u, v) \in \Sigma$  for all  $0 < t \leq T$ .

The function  $f_1(u, v)$  is defined to be quasimonotone nondecreasing if  $f_1$  is nondecreasing for fixed  $v$ . Similarly,  $f_2(u, v)$  is defined to be quasimonotone nondecreasing (resp., nonincreasing) if  $f_2$  is nondecreasing for fixed  $u$ . Quasimonotone nonincreasing is defined similarly.

**Definition 2.2. (Quasimonotone function)** For a vector of function  $\mathbf{f} = (f_1, f_2)$  of two components, there are three basic types of quasimonotone functions: if both  $f_1$  and  $f_2$  are quasimonotone nondecreasing (resp., nonincreasing) for  $(u, v) \in \Sigma$ , then  $\mathbf{f}$  is quasimonotone nondecreasing (resp., nonincreasing); if one of  $f_1$  and  $f_2$  is quasimonotone nonincreasing, and the other one is nondecreasing in  $\Sigma$ , then  $\mathbf{f}$  is mixed quasimonotone.

**Definition 2.3. (Lipschitz continuous)** A vector function  $\mathbf{f} = (f_1, f_2)$  is Lipschitz continuous in  $\Sigma$  when the following condition is satisfied: There exists a constant  $\lambda > 0$  such that for any  $(u_1, v_1), (u_2, v_2) \in \Sigma$ , it holds that

$$\begin{aligned} |f_1(u_1, v_1) - f_1(u_2, v_2)| &\leq \lambda(|u_1 - u_2| + |v_1 - v_2|), \\ |f_2(u_1, v_1) - f_2(u_2, v_2)| &\leq \lambda(|u_1 - u_2| + |v_1 - v_2|). \end{aligned}$$

The following lemma demonstrates that the quasimonotone reaction-diffusion systems possess the invariant region property under certain hypotheses, whose proof can be found in [6].

**Lemma 2.1.** *Suppose  $\kappa_1, \kappa_2 \in [L^\infty(Q_T)]^{2 \times 2}$  are uniformly positive definite in  $Q_T$ ,  $(u_0, v_0) \in [H^1(\Omega)]^2$  and there exists  $(G_1, G_2) \in [W^{2,1}(Q_T)]^2$  such that  $(G_1, G_2)|_{S_T} = (g_1, g_2)$ . Denote  $\Sigma = [m_1, M_1] \times [m_2, M_2]$ , where  $m_1, M_1, m_2, M_2$  are constants. Suppose  $(u_0, v_0)$  and  $(g_1, g_2) \in \Sigma$ ,  $\mathbf{f} = (f_1, f_2)$  is quasimonotone and Lipschitz continuous in  $\Sigma$  and satisfies the following relations*

$$f_1(m_1, v) \geq 0, \quad f_1(M_1, v) \leq 0, \quad f_2(u, m_2) \geq 0, \quad f_2(u, M_2) \leq 0, \quad \forall (u, v) \in \Sigma, \quad (2.3)$$

then the coupled system (2.1)-(2.2) has a weak solution  $(u, v) \in \Sigma$  in  $[W_2^{1,1}(Q_T) \cap L^\infty(Q_T)]^2$  and is unique in  $\Sigma$ .

**Remark 2.1.** (1) When  $\mathbf{f}$  is quasimonotone nondecreasing, the condition (2.3) is equivalent to  $f_1(m_1, m_2) \geq 0, f_1(M_1, M_2) \leq 0, f_2(m_1, m_2) \geq 0, f_2(M_1, M_2) \leq 0$ ;

(2) when  $\mathbf{f}$  is quasimonotone nonincreasing, the condition (2.3) is equivalent to  $f_1(m_1, M_2) \geq 0, f_1(M_1, m_2) \leq 0, f_2(M_1, m_2) \geq 0, f_2(m_1, M_2) \leq 0$ ;

(3) when  $\mathbf{f}$  is mixed quasimonotone with nonincreasing  $f_1$  and nondecreasing  $f_2$ , the condition (2.3) is equivalent to  $f_1(m_1, M_2) \geq 0, f_1(M_1, m_2) \leq 0, f_2(m_1, m_2) \geq 0, f_2(M_1, M_2) \leq 0$ ;

(4) when  $\mathbf{f}$  is mixed quasimonotone with nondecreasing  $f_1$  and nonincreasing  $f_2$ , the condition (2.3) is equivalent to  $f_1(m_1, m_2) \geq 0, f_1(M_1, M_2) \leq 0, f_2(M_1, m_2) \geq 0, f_2(m_1, M_2) \leq 0$ .

### 3 The IRP-preserving finite volume scheme

In this section, an IRP-preserving finite volume scheme is constructed to solve the coupled semilinear parabolic equations (2.1)-(2.2). The numerical method uses DMP-preserving finite volume method in space and backward Euler method in time, and the nonlinear IRP-preserving scheme is obtained.

In order to present the numerical scheme, it is necessary to introduce the following notations, as indicated in Table. 1 and Fig. 3. We suppose that each polygonal cell is star-shaped with respect to its cell-center.

Table 1: The notations.

$K$ or $L$	the cell or the cell-center
$A$ or $B$	the vertex of the cell-edge
$m(K)$	the area of cell $K$
$h$	the maximum diameter of all cells
$\sigma$	the cell-edge
$ \sigma $	the length of $\sigma$
$I$	the midpoint of $\sigma$
$\mathcal{J}_{in}$	the set of cells
$\mathcal{J}_{out}$	the set of cell-edges on $\partial\Omega$
$\mathcal{J}$	$\mathcal{J} = \mathcal{J}_{in} \cup \mathcal{J}_{out}$
$\mathcal{E}_K$	the set of cell-edges of $K$
$\mathcal{E}$	the set of all cell-edges
$\mathbf{n}_{K,\sigma}$	the unit outward normal vector on $\sigma$ of cell $K$
$\boldsymbol{\tau}_{KI}$ (resp. $\boldsymbol{\tau}_{LI}$ )	the unit tangential vector of $KI$ (resp. $LI$ )
$\boldsymbol{\nu}_{KI}$ (resp. $\boldsymbol{\nu}_{LI}$ )	the unit normal vector of $KI$ (resp. $LI$ )
$\theta_{K,\sigma}$ (resp. $\theta_{L,\sigma}$ )	the angle between vectors $\boldsymbol{\tau}_{KI}$ and $\mathbf{n}_{K,\sigma}$ (resp. $\boldsymbol{\tau}_{LI}$ and $\mathbf{n}_{L,\sigma}$ )
$t^{n+1}$	$t^{n+1} = (n+1)\Delta t$ , $\Delta t = \frac{T}{N}$
$\mathcal{F}_{K,\sigma}^{n+1}$ (resp. $\mathcal{F}_{L,\sigma}^{n+1}$ )	the continuous normal flux of $u$ on edge $\sigma$ of the cell $K$ at $t^{n+1}$ (resp. $L$ )
$\tilde{\mathcal{F}}_{K,\sigma}^{n+1}$ (resp. $\tilde{\mathcal{F}}_{L,\sigma}^{n+1}$ )	the continuous normal flux of $v$ on edge $\sigma$ of the cell $K$ at $t^{n+1}$ (resp. $L$ )
$F_{K,\sigma}^{n+1}$ (resp. $F_{L,\sigma}^{n+1}$ )	the discrete normal flux of $u$ on edge $\sigma$ of the cell $K$ at $t^{n+1}$ (resp. $L$ )
$\tilde{F}_{K,\sigma}^{n+1}$ (resp. $\tilde{F}_{L,\sigma}^{n+1}$ )	the discrete normal flux of $v$ on edge $\sigma$ of the cell $K$ at $t^{n+1}$ (resp. $L$ )
$U_X^{n+1}$ ( $X = K, L, A, B, I, \dots$ )	the discrete solution $U$ defined at the point $X$ at $t^{n+1}$
$V_X^{n+1}$ ( $X = K, L, A, B, I, \dots$ )	the discrete solution $V$ defined at the point $X$ at $t^{n+1}$

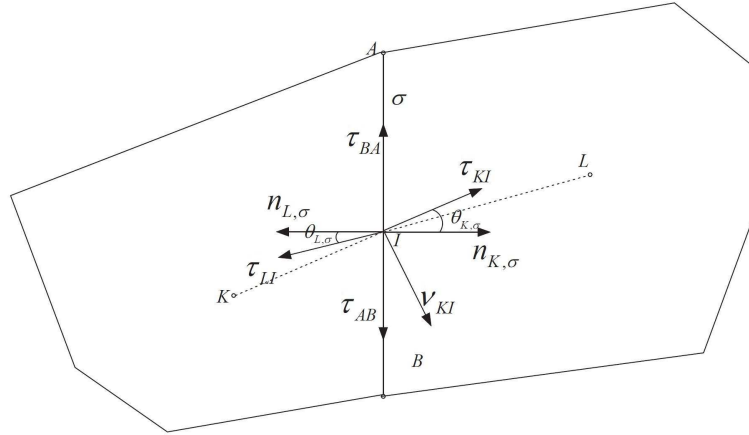


Figure 1: The notations

Integrating the diffusion parts of (2.1)-(2.2) over cell  $K$  at  $t^{n+1}$  and using Green's formula gives

$$\begin{aligned} -\int_K \nabla \cdot (\kappa_1 \nabla u) \Big|_{t=t^{n+1}} \mathrm{d}\mathbf{x} &= \sum_{\sigma \in \mathcal{E}_K} \mathcal{F}_{K,\sigma}^{n+1}, \\ -\int_K \nabla \cdot (\kappa_2 \nabla v) \Big|_{t=t^{n+1}} \mathrm{d}\mathbf{x} &= \sum_{\sigma \in \mathcal{E}_K} \tilde{\mathcal{F}}_{K,\sigma}^{n+1}, \end{aligned}$$

where  $\mathcal{F}_{K,\sigma}^{n+1} = -\int_{\sigma} (\mathbf{n}_{K,\sigma} \cdot \kappa_1^{\top} \nabla u) \Big|_{t=t^{n+1}} \mathrm{d}l$  and  $\tilde{\mathcal{F}}_{K,\sigma}^{n+1} = -\int_{\sigma} (\mathbf{n}_{K,\sigma} \cdot \kappa_2^{\top} \nabla v) \Big|_{t=t^{n+1}} \mathrm{d}l$  represent the continuous normal flux on edge  $\sigma$  for  $u$  and  $v$ , respectively.

Next, we give the discretization of  $\mathcal{F}_{K,\sigma}^{n+1}$ . The discretization of  $\tilde{\mathcal{F}}_{K,\sigma}^{n+1}$  is similar, which is omitted. Without ambiguity, the superscript  $n+1$  is also omitted in the rest of this section. We employ the DMP-preserving numerical fluxes proposed in [16], where the numerical fluxes are both nonlinear and conservative. The vector  $\kappa_1^{\top} \mathbf{n}_{K,\sigma}$  can be decomposed into  $\kappa_1^{\top} \mathbf{n}_{K,\sigma} = -\alpha_K \boldsymbol{\tau}_{BA} + \beta_K \boldsymbol{\tau}_{KI}$ , where  $\theta_{K,\sigma} \in (-\frac{\pi}{2}, \frac{\pi}{2})$  denotes the angle between vectors  $\boldsymbol{\tau}_{KI}$  and  $\mathbf{n}_{K,\sigma}$ ,  $\alpha_K = \frac{1}{\cos \theta_{K,\sigma}} \boldsymbol{\nu}_{KI} \cdot (\kappa_1^{\top} \mathbf{n}_{K,\sigma})$ ,  $\beta_K = \frac{1}{\cos \theta_{K,\sigma}} \mathbf{n}_{K,\sigma} \cdot (\kappa_1^{\top} \mathbf{n}_{K,\sigma})$ ,  $\alpha_L = \frac{1}{\cos \theta_{L,\sigma}} \boldsymbol{\nu}_{LI} \cdot (\kappa_1^{\top} \mathbf{n}_{L,\sigma})$ ,  $\beta_L = \frac{1}{\cos \theta_{L,\sigma}} \mathbf{n}_{L,\sigma} \cdot (\kappa_1^{\top} \mathbf{n}_{L,\sigma})$ . Using Taylor expansion, we obtain

$$\begin{aligned} \mathcal{F}_{K,\sigma} &= \alpha_{K,\sigma} (u(A) - u(B)) - \frac{|AB|}{|IK|} \beta_{K,\sigma} (u(I) - u(K)) + O(h^2), \\ \mathcal{F}_{L,\sigma} &= \alpha_{L,\sigma} (u(B) - u(A)) - \frac{|AB|}{|IL|} \beta_{L,\sigma} (u(I) - u(L)) + O(h^2). \end{aligned} \quad (3.1)$$

$\alpha_{K,\sigma}$ ,  $\alpha_{L,\sigma}$ ,  $\beta_{K,\sigma}$  and  $\beta_{L,\sigma}$  are the integral means of  $\alpha_K$ ,  $\alpha_L$ ,  $\beta_K$  and  $\beta_L$  on edge  $\sigma$ , respectively,

With the help of the continuity of normal flux  $\mathcal{F}_{K,\sigma} + \mathcal{F}_{L,\sigma} = 0$  and omitting the  $O(h^2)$  of  $\mathcal{F}_{K,\sigma}$  and  $\mathcal{F}_{L,\sigma}$  derives the expression of  $u(I)$ , and then substituting  $u(I)$  into (3.1) leads to

$$\begin{aligned} \mathcal{F}_{K,\sigma} &= \tau_{\sigma} (u(K) - u(L)) + \tau_{\sigma} D_{\sigma} (u(A) - u(B)) + O(h^2), \\ \mathcal{F}_{L,\sigma} &= \tau_{\sigma} (u(L) - u(K)) + \tau_{\sigma} D_{\sigma} (u(B) - u(A)) + O(h^2), \end{aligned} \quad (3.2)$$

where  $\tau_{\sigma} = \frac{|AB|}{\frac{|IK|}{\beta_{K,\sigma}} + \frac{|IL|}{\beta_{L,\sigma}}}$ ,  $D_{\sigma} = \frac{|IK| \alpha_{K,\sigma}}{|AB| \beta_{K,\sigma}} + \frac{|IL| \alpha_{L,\sigma}}{|AB| \beta_{L,\sigma}}$ . It can be seen that  $\tau_{\sigma} > 0$  since  $\beta_K > 0$ , but  $D_{\sigma}$  may be negative where its sign depends on the diffusion tensor and mesh cell-geometry.

Using the second-order method in [15] to approximate the vertex unknowns  $u(A)$  and  $u(B)$ , it follows that

$$\begin{aligned} u(A) &= \sum_{i=1}^{J_A} \omega_{A_i} u(K_{A_i}), \\ u(B) &= \sum_{i=1}^{J_B} \omega_{B_i} u(K_{B_i}), \end{aligned}$$

where  $J_A$  (resp.  $J_B$ ) denotes the number of cells involved in the approximation of  $u(A)$  (resp.  $u(B)$ ). The weighted coefficients satisfy  $\sum_{i=1}^{J_A} \omega_{A_i} = 1$  and  $\sum_{i=1}^{J_B} \omega_{B_i} = 1$ , and are not limited to be nonnegative.

Substituting the expressions of  $u(A)$  and  $u(B)$  into (3.2) yields the following expressions

$$\begin{aligned}\mathcal{F}_{K,\sigma} &= \tau_\sigma(u(K) - u(L)) + \tau_\sigma D_\sigma \left( \sum_{i=1}^{J_A} \omega_{A_i} u(K_{A_i}) - \sum_{i=1}^{J_B} \omega_{B_i} u(K_{B_i}) \right) + O(h^2), \\ \mathcal{F}_{L,\sigma} &= \tau_\sigma(u(L) - u(K)) - \tau_\sigma D_\sigma \left( \sum_{i=1}^{J_A} \omega_{A_i} u(K_{A_i}) - \sum_{i=1}^{J_B} \omega_{B_i} u(K_{B_i}) \right) + O(h^2).\end{aligned}$$

Denote by  $F_{K,\sigma}^{NP}$  and  $F_{L,\sigma}^{NP}$  the numerical fluxes of the nine-point scheme [15], we have

$$\begin{aligned}F_{K,\sigma}^{NP} &= \tau_\sigma(U_K - U_L) + \Delta_\sigma, \\ F_{L,\sigma}^{NP} &= \tau_\sigma(U_L - U_K) - \Delta_\sigma,\end{aligned}\tag{3.3}$$

where  $\Delta_\sigma = \tau_\sigma D_\sigma \left( \sum_{i=1}^{J_A} \omega_{A_i} U_{K_{A_i}} - \sum_{i=1}^{J_B} \omega_{B_i} U_{K_{B_i}} \right)$ ,  $U$  represents the discrete solution.

Denote  $U_{K_1}$  and  $U_{K_2}$  such that

$$\begin{aligned}U_{K_1} &= \min_{\bar{K} \in \mathcal{J}_K} U_{\bar{K}}, \\ U_{K_2} &= \max_{\bar{K} \in \mathcal{J}_K} U_{\bar{K}},\end{aligned}\tag{3.4}$$

where  $\mathcal{J}_K$  denotes the set of cells that have common vertices with cell  $K$  except for  $K$ .

In the numerical algorithm, we set two small positive constants  $\varepsilon_0$  and  $\varepsilon_1$ , where  $\varepsilon_0, \varepsilon_1 \leq Ch^2$ . We set  $\varepsilon_0 = \varepsilon_1 = 10^{-10}$  in our numerical experiments.

If  $|\Delta_\sigma| \leq \varepsilon_0$ , we define the numerical fluxes as follows:

$$\begin{aligned}F_{K,\sigma} &= \tau_\sigma(U_K - U_L), \\ F_{L,\sigma} &= \tau_\sigma(U_L - U_K).\end{aligned}$$

If  $|\Delta_\sigma| > \varepsilon_0$ , then the construction contains two cases:

**Case 1.** There exist  $U_{K'}$  and  $U_{L'}$  such that

$$\begin{aligned}\Delta_\sigma(U_K - U_{K'}) &> 0, \\ \Delta_\sigma(U_{L'} - U_L) &> 0,\end{aligned}\tag{3.5}$$

where  $U_{K'}$  and  $U_{L'}$  are the cell-centered unknowns surrounding  $K$  and  $L$ , respectively.  $U_{K'}$  and  $U_{L'}$  can be taken as  $U_{K_1}$  or  $U_{K_2}$  in (3.4). In this case, the numerical fluxes are defined as

$$\begin{aligned}F_{K,\sigma} &= \tau_\sigma(U_K - U_L) + \eta_{K,\sigma}(U_K - U_{K'}), \\ F_{L,\sigma} &= \tau_\sigma(U_L - U_K) + \eta_{L,\sigma}(U_L - U_{L'}),\end{aligned}$$

where  $\eta_{K,\sigma} = \frac{\Delta_\sigma}{U_K - U_{K'}}$  and  $\eta_{L,\sigma} = \frac{\Delta_\sigma}{U_{L'} - U_L}$ . It can be obtained that the nonlinear coefficients  $\eta_{K,\sigma} > 0$  and  $\eta_{L,\sigma} > 0$  since  $\Delta_\sigma$  and  $U_K - U_{K'}$ ,  $U_{L'} - U_L$  are of the same sign in this case.

**Case 2.** There do not exist  $U_{K'}$  and  $U_{L'}$  such that (3.5) hold. It is equivalent to

$$\Delta_\sigma(U_K - U_{K'}) \leq 0 \quad (3.6)$$

for any  $K' \in \mathcal{J}_K$ , or

$$\Delta_\sigma(U_{L'} - U_L) \leq 0 \quad (3.7)$$

for any  $L' \in \mathcal{J}_L$ . It implies that  $U$  reaches its maximum or minimum on cell  $K$  or  $L$ , and from (3.6) and (3.7) we have

$$\Delta_\sigma(U_K - U_L) \leq 0. \quad (3.8)$$

Rewrite the linear numerical fluxes (3.3) as

$$\begin{aligned} F_{K,\sigma}^{NP} &= (1 - \gamma_0)\tau_\sigma(U_K - U_L) + \Delta_\sigma + \gamma_0\tau_\sigma(U_K - U_L), \\ F_{L,\sigma}^{NP} &= (1 - \gamma_0)\tau_\sigma(U_L - U_K) - \Delta_\sigma + \gamma_0\tau_\sigma(U_L - U_K), \end{aligned}$$

where  $\gamma_0$  is a nonlinear coefficient determined later. To preserve the IRP, the numerical flux needs to satisfy the DMP structure, i.e., the numerical flux should be the convex combinations of  $U_K - U_{K_j}$ . To guarantee  $1 - \gamma_0 > 0$ , the coefficient  $\gamma_0$  should satisfy

$$0 \leq \gamma_0 \leq 1 - \varepsilon_1.$$

In this case, we define the final nonlinear numerical fluxes:

$$\begin{aligned} F_{K,\sigma} &= (1 - \gamma_0)\tau_\sigma(U_K - U_L), \\ F_{L,\sigma} &= (1 - \gamma_0)\tau_\sigma(U_L - U_K). \end{aligned}$$

If  $|U_K - U_L| = 0$ , we set  $\gamma_0 = 1 - \varepsilon_1$ , otherwise, we set

$$\gamma_0 = \begin{cases} \frac{-\Delta_\sigma}{\tau_\sigma(U_K - U_L)}, & \text{if } \frac{-\Delta_\sigma}{\tau_\sigma(U_K - U_L)} \leq 1 - \varepsilon_1, \\ 1 - \varepsilon_1, & \text{else.} \end{cases}$$

The inequality (3.8) guarantees the nonnegativity of  $\gamma_0$ .

Up to now we have constructed the numerical flux with DMP-preserving structure, where the numerical flux is conservative and nonlinear.



To discretize the time derivative, we utilize the Backward Euler method. Hence, we obtain the nonlinear finite volume scheme (3.9)-(3.14):

$$m(K) \frac{U_K^{n+1} - U_K^n}{\Delta t} + \sum_{\sigma \in \mathcal{E}_K} F_{K,\sigma}^{n+1} = m(K) f_1(U_K^{n+1}, V_K^{n+1}), \quad \forall K \in \mathcal{J}_{in}, \quad (3.9)$$

$$m(K) \frac{V_K^{n+1} - V_K^n}{\Delta t} + \sum_{\sigma \in \mathcal{E}_K} \tilde{F}_{K,\sigma}^{n+1} = m(K) f_2(U_K^{n+1}, V_K^{n+1}), \quad \forall K \in \mathcal{J}_{in}, \quad (3.10)$$

$$U_K^{n+1} = g_1(K, t^{n+1}), \quad \forall K \in \mathcal{J}_{out}, \quad (3.11)$$

$$V_K^{n+1} = g_2(K, t^{n+1}), \quad \forall K \in \mathcal{J}_{out}, \quad (3.12)$$

$$U_K^0 = u_0(K), \quad \forall K \in \mathcal{J}_{in} \cup \mathcal{J}_{out}, \quad (3.13)$$

$$V_K^0 = v_0(K), \quad \forall K \in \mathcal{J}_{in} \cup \mathcal{J}_{out}. \quad (3.14)$$

We show that the finite volume scheme (3.9)-(3.14) can preserve the IRP for the semi-linear parabolic systems with three basic types of quasimonotone functions, which are shown in Theorem 3.1 and Theorem 3.2.

**Theorem 3.1.** *Assume that  $\mathbf{f} = (f_1, f_2)$  is mixed quasimonotone and Lipschitz continuous in  $\Sigma = [m_1, M_1] \times [m_2, M_2]$  and satisfies (2.3), the initial and boundary conditions satisfy  $(u_0, v_0), (g_1, g_2) \in \Sigma$ . When the time-step size satisfies  $\Delta t < \frac{1}{\lambda}$ , the finite volume scheme (3.9)-(3.14) has a solution satisfying*

$$(U_K^n, V_K^n) \in \Sigma, \quad \forall K \in \mathcal{J}, \quad 0 \leq n \leq N. \quad (3.15)$$

*Proof.* This theorem is proved by induction. For mixed quasimonotone reaction-diffusion systems, we only prove the theorem in the case that  $f_1$  is quasimonotone nonincreasing and  $f_2$  is quasimonotone nondecreasing, the other case can be proved similarly. Since  $(u_0, v_0), (g_1, g_2) \in \Sigma$ , it is obvious that (3.15) holds for  $n = 0$ . Suppose that (3.15) holds for any  $n \leq m$ , if (3.15) is proved for  $n = m+1$ , where  $m \geq 0$ , then the theorem follows immediately.

First, construct the prolongation functions  $\tilde{f}_1(u_1, u_2)$  and  $\tilde{f}_2(u_1, u_2)$  as follows. For any  $u_1 \in \mathbb{R}$ , define

$$\tilde{f}_1(u_1, u_2) = \begin{cases} f_1(u_1, m_2), & \text{if } u_2 < m_1, \\ f_1(u_1, u_2), & \text{if } m_2 \leq u_2 \leq M_2, \\ f_1(u_1, M_2), & \text{if } u_2 > M_2. \end{cases}$$

For any  $u_2 \in \mathbb{R}$ , define

$$\tilde{f}_2(u_1, u_2) = \begin{cases} f_2(m_1, u_2), & \text{if } u_1 < m_1, \\ f_2(u_1, u_2), & \text{if } m_1 \leq u_1 \leq M_1, \\ f_2(M_1, u_2), & \text{if } u_1 > M_1. \end{cases}$$

Note that  $(\bar{f}_1, \bar{f}_2)$  is also mixed quasimonotone in  $\mathbb{R}^2$ . It is easy to check that  $\bar{f}_1$  and  $\bar{f}_2$  are Lipschitz continuous in  $\mathbb{R}^2$  and  $\lambda$  is still the Lipschitz constant of  $\bar{f}_1$  and  $\bar{f}_2$ , and it also holds that

$$\begin{aligned}\bar{f}_1(M_1, m_2) &\leq 0 \leq \bar{f}_1(m_1, M_2), \\ \bar{f}_2(M_1, M_2) &\leq 0 \leq \bar{f}_2(m_1, m_2).\end{aligned}$$

Next, for given  $(U^m, V^m) \in \Sigma$ , denote  $(\bar{U}^{m+1}, \bar{V}^{m+1})$  the solution of following problem:

$$m(K) \frac{\bar{U}_K^{m+1} - U_K^m}{\Delta t} + \sum_{\sigma \in \mathcal{E}_K} F_{K,\sigma}^{m+1} = m(K) \bar{f}_1(\bar{U}_K^{m+1}, \bar{V}_K^{m+1}), \quad \forall K \in \mathcal{J}_{in}, \quad (3.16)$$

$$m(K) \frac{\bar{V}_K^{m+1} - V_K^m}{\Delta t} + \sum_{\sigma \in \mathcal{E}_K} \tilde{F}_{K,\sigma}^{m+1} = m(K) \bar{f}_2(\bar{U}_K^{m+1}, \bar{V}_K^{m+1}), \quad \forall K \in \mathcal{J}_{in}, \quad (3.17)$$

$$\bar{U}_K^{m+1} = g_1(K, t^{m+1}), \quad \forall K \in \mathcal{J}_{out}, \quad (3.18)$$

$$\bar{V}_K^{m+1} = g_2(K, t^{m+1}), \quad \forall K \in \mathcal{J}_{out}, \quad (3.19)$$

where  $F_{K,\sigma}^{m+1}$  and  $\tilde{F}_{K,\sigma}^{m+1}$  are constructed by  $\bar{U}_K^{m+1}$  and  $\bar{V}_K^{m+1}$ .

Denote  $K_{\max,U}$ ,  $K_{\min,U}$ ,  $K_{\max,V}$ ,  $K_{\min,V}$  such that

$$\begin{aligned}\bar{U}_{K_{\max,U}}^{m+1} &= \max_{K \in \mathcal{J}} \bar{U}_K^{m+1}, & \bar{U}_{K_{\min,U}}^{m+1} &= \min_{K \in \mathcal{J}} \bar{U}_K^{m+1}, \\ \bar{V}_{K_{\max,V}}^{m+1} &= \max_{K \in \mathcal{J}} \bar{V}_K^{m+1}, & \bar{V}_{K_{\min,V}}^{m+1} &= \min_{K \in \mathcal{J}} \bar{V}_K^{m+1}.\end{aligned}$$

If (3.15) does not hold for  $n = m + 1$ , then one of the following cases holds:

$$\begin{aligned}\text{Case 1: } & \bar{U}_{K_{\max,U}}^{m+1} > M_1. & \text{Case 2: } & \bar{U}_{K_{\min,U}}^{m+1} < m_1. \\ \text{Case 3: } & \bar{V}_{K_{\max,V}}^{m+1} > M_2. & \text{Case 4: } & \bar{V}_{K_{\min,V}}^{m+1} < m_2.\end{aligned}$$

We shall prove that none of the above cases hold true by contradiction. Let us suppose Case 1 holds. Since  $\bar{U}^{m+1}$  attains its maximum on  $K_{\max,U}$  and the numerical flux has DMP-preserving structure, it holds that  $F_{K_{\max,U},\sigma}^{m+1} \leq 0$  for any  $\sigma \in \mathcal{E}_{K_{\max,U}}$ . From  $U_{K_{\max,U}}^m \in [m_1, M_1]$  and (3.9), we can get

$$\frac{\bar{U}_{K_{\max,U}}^{m+1} - M_1}{\Delta t} \leq \frac{\bar{U}_{K_{\max,U}}^{m+1} - U_{K_{\max,U}}^m}{\Delta t} \leq \bar{f}_1(\bar{U}_{K_{\max,U}}^{m+1}, \bar{V}_{K_{\max,U}}^{m+1}). \quad (3.20)$$

$$(1) \bar{V}_{K_{\max,U}}^{m+1} \geq m_2.$$

Since  $\bar{f}_1$  is nonincreasing with respect to  $v$ , we have  $\bar{f}_1(M_1, \bar{V}_{K_{\max,U}}^{m+1}) \leq \bar{f}_1(M_1, m_2) \leq 0$ .

According to (3.20) and Lipschitz continuity of  $\bar{f}_1$ , we have

$$\frac{\bar{U}_{K_{\max,U}}^{m+1} - M_1}{\Delta t} \leq \bar{f}_1(\bar{U}_{K_{\max,U}}^{m+1}, \bar{V}_{K_{\max,U}}^{m+1}) - \bar{f}_1(M_1, \bar{V}_{K_{\max,U}}^{m+1}) \leq \lambda(\bar{U}_{K_{\max,U}}^{m+1} - M_1). \quad (3.21)$$

When  $\Delta t < \frac{1}{\lambda}$ , (3.21) implies that  $\bar{U}_{K_{\max,U}}^{m+1} \leq M_1$ , which contradicts with the assumption that  $\bar{U}_{K_{\max,U}}^{m+1} > M_1$ .

$$(2) \bar{V}_{K_{\max,U}}^{m+1} < m_2.$$

From  $\bar{V}_{K_{\max,U}}^{m+1} < m_2$ , we have  $\bar{V}_{K_{\min,V}}^{m+1} < m_2$ . Since  $\bar{V}^{m+1}$  attains its minimum on  $K_{\min,V}$ , we can obtain

$$\frac{\bar{V}_{K_{\min,V}}^{m+1} - m_2}{\Delta t} \geq \frac{\bar{V}_{K_{\min,V}}^{m+1} - \bar{V}_{K_{\min,V}}^m}{\Delta t} \geq \bar{f}_2(\bar{U}_{K_{\min,V}}^{m+1}, \bar{V}_{K_{\min,V}}^{m+1}). \quad (3.22)$$

$$(2.1) \bar{U}_{K_{\min,V}}^{m+1} \geq m_1.$$

Since  $\bar{f}_2$  is nondecreasing with respect to  $u$ , we have  $\bar{f}_2(\bar{U}_{K_{\min,U}}^{m+1}, m_2) \geq \bar{f}_2(m_1, m_2) \geq 0$ . Similar to the derivation of (3.21), it follows that

$$\frac{\bar{V}_{K_{\min,V}}^{m+1} - m_2}{\Delta t} \geq \bar{f}_2(\bar{U}_{K_{\min,V}}^{m+1}, \bar{V}_{K_{\min,V}}^{m+1}) - \bar{f}_2(\bar{U}_{K_{\min,U}}^{m+1}, m_2) \geq \lambda(\bar{V}_{K_{\min,V}}^{m+1} - m_2). \quad (3.23)$$

When  $\Delta t < \frac{1}{\lambda}$ , (3.23) implies  $\bar{V}_{K_{\min,V}}^{m+1} \geq m_2$ , which contradicts with  $\bar{V}_{K_{\min,V}}^{m+1} < m_2$ .

$$(2.2) \bar{U}_{K_{\min,V}}^{m+1} < m_1.$$

The assumption  $\bar{U}_{K_{\min,V}}^{m+1} < m_1$  implies  $\bar{U}_{K_{\min,U}}^{m+1} < m_1$ . Since  $\bar{U}^{m+1}$  attains its minimum on  $K_{\min,U}$ , we can obtain

$$\frac{\bar{U}_{K_{\min,U}}^{m+1} - m_1}{\Delta t} \geq \frac{\bar{U}_{K_{\min,U}}^{m+1} - \bar{U}_{K_{\min,U}}^m}{\Delta t} \geq \bar{f}_1(\bar{U}_{K_{\min,U}}^{m+1}, \bar{V}_{K_{\min,U}}^{m+1}). \quad (3.24)$$

$$(2.2.1) \bar{V}_{K_{\min,U}}^{m+1} \leq M_2.$$

Since  $\bar{f}_1$  is nonincreasing with respect to  $v$ , we have  $\bar{f}_1(m_1, \bar{V}_{K_{\min,U}}^{m+1}) \geq \bar{f}_1(m_1, M_2) \geq 0$ . According to (3.24) and the Lipschitz continuity of  $\bar{f}_1$ , we have

$$\frac{\bar{U}_{K_{\min,U}}^{m+1} - m_1}{\Delta t} \geq \bar{f}_1(\bar{U}_{K_{\min,U}}^{m+1}, \bar{V}_{K_{\min,U}}^{m+1}) - \bar{f}_1(m_1, \bar{V}_{K_{\min,U}}^{m+1}) \geq \lambda(\bar{U}_{K_{\min,U}}^{m+1} - m_1),$$

which means that  $\bar{U}_{K_{\min,U}}^{m+1} \geq m_1$  when  $\Delta t < \frac{1}{\lambda}$ . This contradicts with  $\bar{U}_{K_{\min,U}}^{m+1} < m_1$ .

$$(2.2.2) \bar{V}_{K_{\min,U}}^{m+1} > M_2.$$

The assumption  $\bar{V}_{K_{\min,U}}^{m+1} > M_2$  implies  $\bar{V}_{K_{\max,V}}^{m+1} > M_2$ . Since  $\bar{V}^{m+1}$  attains its maximum on  $K_{\max,V}$ , we can obtain

$$\frac{\bar{V}_{K_{\max,V}}^{m+1} - M_2}{\Delta t} \leq \frac{\bar{V}_{K_{\max,V}}^{m+1} - \bar{V}_{K_{\max,V}}^m}{\Delta t} \leq \bar{f}_2(\bar{U}_{K_{\max,V}}^{m+1}, \bar{V}_{K_{\max,V}}^{m+1}). \quad (3.25)$$

$$(2.2.2.1) \bar{U}_{K_{\max,V}}^{m+1} \leq M_1.$$

Since  $\bar{f}_2$  is nondecreasing with respect to  $u$ , we have  $\bar{f}_2(\bar{U}_{K_{\max,V}}^{m+1}, M_2) \leq \bar{f}_2(M_1, M_2) \leq 0$ . According to (3.25) and the Lipschitz continuity of  $\bar{f}_2$ , we have

$$\frac{\bar{V}_{K_{\max,V}}^{m+1} - M_2}{\Delta t} \leq \bar{f}_2(\bar{U}_{K_{\max,V}}^{m+1}, \bar{V}_{K_{\max,V}}^{m+1}) - \bar{f}_2(\bar{U}_{K_{\max,V}}^{m+1}, M_2) \leq \lambda(\bar{V}_{K_{\max,V}}^{m+1} - M_2), \quad (3.26)$$

which means  $\bar{V}_{K_{\max,V}}^{m+1} \leq M_2$  provided that  $\Delta t < \frac{1}{\lambda}$ . This contradicts with  $\bar{V}_{K_{\max,V}}^{m+1} > M_2$ .

$$(2.2.2.2) \quad \bar{U}_{K_{\max,U}}^{m+1} > M_1.$$

Since  $\bar{f}_1$  is nonincreasing with respect to  $v$  and  $\bar{V}_{K_{\max,U}}^{m+1} > M_2 > m_2$ , we have  $\bar{f}_1(M_1, \bar{V}_{K_{\max,U}}^{m+1}) \leq \bar{f}_1(M_1, m_2) \leq 0$ . Similar to the derivation of (3.21), it holds that

$$\frac{\bar{U}_{K_{\max,U}}^{m+1} - M_1}{\Delta t} \leq \lambda(\bar{U}_{K_{\max,U}}^{m+1} - M_1),$$

which implies  $\bar{U}_{K_{\max,U}}^{m+1} \leq M_1$  provided that  $\Delta t < \frac{1}{\lambda}$ . This contradicts with  $\bar{U}_{K_{\max,U}}^{m+1} > M_1$ .

In conclusion, Case 1 does not hold provided that  $\Delta t < \frac{1}{\lambda}$ . Similarly, the other cases do not hold when  $\Delta t < \frac{1}{\lambda}$ . Hence  $(\bar{U}_K^{m+1}, \bar{V}_K^{m+1}) \in \Sigma$  for any  $K \in \mathcal{J}_{in} \cup \mathcal{J}_{out}$ , it follows that  $\bar{f}_1(\bar{U}_K^{m+1}, \bar{V}_K^{m+1}) = f_1(\bar{U}_K^{m+1}, \bar{V}_K^{m+1})$ ,  $\bar{f}_2(\bar{U}_K^{m+1}, \bar{V}_K^{m+1}) = f_2(\bar{U}_K^{m+1}, \bar{V}_K^{m+1})$ . We obtain that  $(\bar{U}_K^{m+1}, \bar{V}_K^{m+1}) \in \Sigma$  is also the solution of following scheme

$$\begin{aligned} m(K) \frac{U_K^{m+1} - U_K^m}{\Delta t} + \sum_{\sigma \in \mathcal{E}_K} F_{K,\sigma}^{m+1} &= m(K) f_1(U_K^{m+1}, V_K^{m+1}), & \forall K \in \mathcal{J}_{in}, \\ m(K) \frac{V_K^{m+1} - V_K^m}{\Delta t} + \sum_{\sigma \in \mathcal{E}_K} \tilde{F}_{K,\sigma}^{m+1} &= m(K) f_2(U_K^{m+1}, V_K^{m+1}), & \forall K \in \mathcal{J}_{in}, \\ U_K^{m+1} &= g_1(K, t^{m+1}), & \forall K \in \mathcal{J}_{out}, \\ V_K^{m+1} &= g_2(K, t^{m+1}), & \forall K \in \mathcal{J}_{out}, \end{aligned}$$

which means that the finite volume scheme (3.9)-(3.14) has a solution  $(U^{m+1}, V^{m+1})$  in the invariant region. This completes the proof.  $\square$

We shall now demonstrate that the finite volume scheme can preserve the IRP for the semilinear parabolic systems with quasimonotone nondecreasing reaction function. The same method can be applied for the case of a quasimonotone nonincreasing reaction function, which we will omit for brevity.

**Theorem 3.2.** *Suppose that  $\mathbf{f} = (f_1, f_2)$  is quasimonotone nondecreasing (or vice versa) and Lipschitz continuous in  $\Sigma = [m_1, M_1] \times [m_2, M_2]$  and satisfies (2.3), the initial and boundary conditions*

satisfy  $(u_0, v_0), (g_1, g_2) \in \Sigma$ . When the time-step size satisfies  $\Delta t < \frac{1}{2\lambda}$ , the finite volume scheme has a solution satisfying

$$(U_K^n, V_K^n) \in \Sigma, \quad \forall K \in \mathcal{J}, \quad 0 \leq n \leq N. \quad (3.27)$$

*Proof.* We shall adopt the same procedure as in the proof of Theorem 3.1. It is obvious that (3.27) holds for  $n = 0$ . Suppose that (3.27) holds for any  $n \leq m$ , where  $m \geq 0$ . Our objective is to demonstrate that (3.27) holds for  $n = m + 1$ .

The definitions of prolongation functions  $\bar{f}_1(u_1, u_2)$  and  $\bar{f}_2(u_1, u_2)$  are the same as in the proof of Theorem 3.1, and  $(\bar{f}_1, \bar{f}_2)$  is also quasimonotone nondecreasing in  $\mathbb{R}^2$  and satisfies

$$\begin{aligned} \bar{f}_1(M_1, M_2) &\leq 0 \leq \bar{f}_1(m_1, m_2), \\ \bar{f}_2(M_1, M_2) &\leq 0 \leq \bar{f}_2(m_1, m_2). \end{aligned}$$

Similar to the proof of Theorem 3.1, we define  $(\bar{U}^{m+1}, \bar{V}^{m+1})$  the solution of the finite volume scheme corresponding to  $(\bar{f}_1, \bar{f}_2)$ . The definitions of  $K_{\max, U}$ ,  $K_{\min, U}$ ,  $K_{\max, V}$  and  $K_{\min, V}$  are also the same as those in Theorem 3.1.

Suppose that (3.27) does not hold for  $n = m + 1$ , then one of the following cases holds:

$$\begin{aligned} \text{Case 1: } \bar{U}_{K_{\max, U}}^{m+1} &> M_1. & \text{Case 2: } \bar{U}_{K_{\min, U}}^{m+1} &< m_1. \\ \text{Case 3: } \bar{V}_{K_{\max, V}}^{m+1} &> M_2. & \text{Case 4: } \bar{V}_{K_{\min, V}}^{m+1} &< m_2. \end{aligned}$$

Let us suppose Case 1 holds. We can obtain that (3.20) holds since  $\bar{U}^{m+1}$  attains its maximum on  $K_{\max, U}$ .

$$(1) \bar{V}_{K_{\max, U}}^{m+1} \leq M_2.$$

Since  $\bar{f}_1$  is nondecreasing with respect to  $v$ , we have  $\bar{f}_1(M_1, \bar{V}_{K_{\max, U}}^{m+1}) \leq \bar{f}_1(M_1, M_2) \leq 0$ . Similar to the derivation of (3.21), we obtain

$$\frac{\bar{U}_{K_{\max, U}}^{m+1} - M_1}{\Delta t} \leq \lambda (\bar{U}_{K_{\max, U}}^{m+1} - M_1). \quad (3.28)$$

(3.28) implies  $\bar{U}_{K_{\max, U}}^{m+1} \leq M_1$  provided that  $\Delta t < \frac{1}{\lambda}$ , this leads to a contradiction with Case 1.

$$(2) \bar{V}_{K_{\max, U}}^{m+1} > M_2.$$

The assumption  $\bar{V}_{K_{\max, U}}^{m+1} > M_2$  implies  $\bar{V}_{K_{\max, V}}^{m+1} > M_2$ . It follows that (3.25) since  $\bar{V}_{K_{\max, V}}^{m+1}$  is the maximum of  $\bar{V}^{m+1}$ .

$$(2.1) \bar{U}_{K_{\max, V}}^{m+1} \leq M_1.$$

Since  $\bar{f}_2$  is nondecreasing with respect to  $u$ , we have  $\bar{f}_2(\bar{U}_{K_{\max, V}}^{m+1}, M_2) \leq \bar{f}_2(M_1, M_2) \leq 0$ . Similar to the derivation of (3.26), we have

$$\frac{\bar{V}_{K_{\max, V}}^{m+1} - M_2}{\Delta t} \leq \lambda (\bar{V}_{K_{\max, V}}^{m+1} - M_2). \quad (3.29)$$

When  $\Delta t < \frac{1}{\lambda}$ , (3.29) implies that  $\bar{V}_{K_{\max,V}}^{m+1} \leq M_2$ , which contradicts with  $\bar{V}_{K_{\max,U}}^{m+1} > M_2$ .

$$(2.2) \quad \bar{U}_{K_{\max,V}}^{m+1} > M_1.$$

The assumption  $\bar{U}_{K_{\max,V}}^{m+1} > M_1$  implies that  $\bar{U}_{K_{\max,U}}^{m+1} > M_1$ . From the Lipschitz continuity of  $\bar{f}_1$  and  $\bar{f}_1(M_1, M_2) \geq 0$ , it follows that

$$\begin{aligned} \frac{\bar{U}_{K_{\max,U}}^{m+1} - M_1}{\Delta t} &\leq \bar{f}_1(\bar{U}_{K_{\max,U}}^{m+1}, \bar{V}_{K_{\max,U}}^{m+1}) - \bar{f}_1(M_1, M_2) \\ &\leq \lambda(\bar{U}_{K_{\max,U}}^{m+1} - M_1) + \lambda(\bar{V}_{K_{\max,U}}^{m+1} - M_2). \end{aligned} \quad (3.30)$$

From (3.30), we can obtain that

$$\bar{U}_{K_{\max,U}}^{m+1} - M_1 \leq \frac{\lambda \Delta t}{1 - \lambda \Delta t} (\bar{V}_{K_{\max,U}}^{m+1} - M_2). \quad (3.31)$$

Similar to the derivations of (3.30) and (3.31),  $\bar{V}_{K_{\max,V}}^{m+1}$  satisfies the following inequalities

$$\begin{aligned} \frac{\bar{V}_{K_{\max,U}}^{m+1} - M_2}{\Delta t} &\leq \bar{f}_2(\bar{U}_{K_{\max,V}}^{m+1}, \bar{V}_{K_{\max,V}}^{m+1}) - \bar{f}_2(M_1, M_2) \\ &\leq \lambda(\bar{U}_{K_{\max,V}}^{m+1} - M_1) + \lambda(\bar{V}_{K_{\max,V}}^{m+1} - M_2), \end{aligned}$$

and

$$\bar{U}_{K_{\max,V}}^{m+1} - M_1 \geq \frac{1 - \lambda \Delta t}{\lambda \Delta t} (\bar{V}_{K_{\max,V}}^{m+1} - M_2). \quad (3.32)$$

Combining (3.31) and (3.32), we see that  $\frac{\lambda \Delta t}{1 - \lambda \Delta t} (\bar{V}_{K_{\max,U}}^{m+1} - M_2) \geq \frac{1 - \lambda \Delta t}{\lambda \Delta t} (\bar{V}_{K_{\max,V}}^{m+1} - M_2)$ .

We have  $\frac{\lambda \Delta t}{1 - \lambda \Delta t} > \frac{1 - \lambda \Delta t}{\lambda \Delta t}$  provided that  $\Delta t < \frac{1}{2\lambda}$ , which derives that  $\bar{V}_{K_{\max,U}}^{m+1} \leq M_2$ . It contradicts with the assumption that  $\bar{V}_{K_{\max,U}}^{m+1} > M_2$ . Hence, Case 1 does not hold when  $\Delta t < \frac{1}{2\lambda}$ . The proofs of other cases follow similarly.

In conclusion, we have proved that  $(\bar{U}_K^{m+1}, \bar{V}_K^{m+1}) \in \Sigma$  for any  $K \in \mathcal{J}_{in} \cup \mathcal{J}_{out}$ , then we have  $\bar{f}_1(\bar{U}_K^{m+1}, \bar{V}_K^{m+1}) = f_1(\bar{U}_K^{m+1}, \bar{V}_K^{m+1})$  and  $\bar{f}_2(\bar{U}_K^{m+1}, \bar{V}_K^{m+1}) = f_2(\bar{U}_K^{m+1}, \bar{V}_K^{m+1})$ . It means that  $(\bar{U}^{m+1}, \bar{V}^{m+1})$  is also the solution of the finite volume scheme (3.9)-(3.14), which completes the proof.  $\square$

The existence of solution for the nonlinear finite volume scheme (3.9)-(3.14) can be established using the same method as Theorem 4 in [19], and so is omitted.

**Theorem 3.3.** *Suppose that  $\mathbf{f} = (f_1, f_2)$  is quasimonotone and Lipschitz continuous in  $\Sigma = [m_1, M_1] \times [m_2, M_2]$ , and satisfies (2.3), the initial and boundary conditions satisfy  $(u_0, v_0), (g_1, g_2) \in \Sigma$ . When  $\Delta t < \frac{1}{2\lambda}$ , the nonlinear finite volume scheme (3.9)-(3.14) has at least one solution.*

## 4 The iterative method preserving the IRP

In this section, we design iterative method to solve the nonlinear scheme (3.9)-(3.14), and then prove the IRP of the iteration. To design the iterative scheme, the nonlinear numerical flux needs to be linearized first. Denote  $U^{n+1,s+1}$  and  $V^{n+1,s+1}$  the  $(s+1)$ -th iterative numerical solutions at  $t^{n+1}$ . We use the solution  $U^{n+1,s}$  to calculate the coefficients  $\eta_{K,\sigma}^{n+1,s}$ ,  $\eta_{L,\sigma}^{n+1,s}$ ,  $\gamma_0^{n+1,s}$  and  $\Delta_\sigma^{n+1,s}$ . For Case 1 in the algorithm, the numerical flux  $F_{K,\sigma}^{n+1,s+1}$  and  $F_{L,\sigma}^{n+1,s+1}$  are defined as

$$\begin{aligned} F_{K,\sigma}^{n+1,s+1} &= \tau_\sigma^{n+1} \left( U_K^{n+1,s+1} - U_L^{n+1,s+1} \right) + \eta_{K,\sigma}^{n+1,s} \left( U_K^{n+1,s+1} - U_{K'}^{n+1,s+1} \right), \\ F_{L,\sigma}^{n+1,s+1} &= \tau_\sigma^{n+1} \left( U_L^{n+1,s+1} - U_K^{n+1,s+1} \right) + \eta_{L,\sigma}^{n+1,s} \left( U_L^{n+1,s+1} - U_{L'}^{n+1,s+1} \right), \end{aligned}$$

and for Case 2,  $F_{K,\sigma}^{n+1,s+1}$  and  $F_{L,\sigma}^{n+1,s+1}$  are defined as

$$\begin{aligned} F_{K,\sigma}^{n+1,s+1} &= (1 - \gamma_0^{n+1,s}) \tau_\sigma^{n+1} \left( U_K^{n+1,s+1} - U_L^{n+1,s+1} \right), \\ F_{L,\sigma}^{n+1,s+1} &= (1 - \gamma_0^{n+1,s}) \tau_\sigma^{n+1} \left( U_L^{n+1,s+1} - U_K^{n+1,s+1} \right). \end{aligned}$$

$\tilde{F}_{K,\sigma}^{n+1,s+1}$  and  $\tilde{F}_{L,\sigma}^{n+1,s+1}$  are defined similarly.

The treatment of the nonlinear source term is crucial for preserving IRP during the iteration. For given  $U^{n+1,s}$  and  $V^{n+1,s}$ , the solution of the iteration  $(U^{n+1,s+1}, V^{n+1,s+1})$  satisfies

$$m(K) \frac{U_K^{n+1,s+1} - U_K^n}{\Delta t} + \sum_{\sigma \in \mathcal{E}_K} F_{K,\sigma}^{n+1,s+1} + \lambda m(K) U_K^{n+1,s+1} = m(K) \left( \lambda U_K^{n+1,s} + f_1(U_K^{n+1,s}, V_K^{n+1,s}) \right), \quad (4.1)$$

$$m(K) \frac{V_K^{n+1,s+1} - V_K^n}{\Delta t} + \sum_{\sigma \in \mathcal{E}_K} \tilde{F}_{K,\sigma}^{n+1,s+1} + \lambda m(K) V_K^{n+1,s+1} = m(K) \left( \lambda V_K^{n+1,s} + f_2(U_K^{n+1,s+1}, V_K^{n+1,s}) \right), \quad (4.2)$$

for any  $K \in \mathcal{J}_{in}$ , and subject to  $U_K^{n+1,s+1} = g_1(K, t^{n+1})$  and  $V_K^{n+1,s+1} = g_2(K, t^{n+1})$  for any  $K \in \mathcal{J}_{out}$ ,  $U_K^0 = u_0(K)$  and  $V_K^0 = v_0(K)$  for any  $K \in \mathcal{J}_{in} \cup \mathcal{J}_{out}$ , where  $n \geq 0$ ,  $s \geq 0$ . The iterative algorithm is described in Algorithm 1, where we set  $\varepsilon = 10^{-8}$  in the numerical experiments.

We prove that the iterative method can preserve the IRP for the coupled quasimonotone parabolic system.

**Theorem 4.1.** *Suppose that  $\mathbf{f} = (f_1, f_2)$  is quasimonotone and Lipschitz continuous in  $\Sigma = [m_1, M_1] \times [m_2, M_2]$  and satisfies (2.3), the initial and boundary conditions satisfy  $(u_0, v_0) \in \Sigma$ ,  $(g_1, g_2) \in \Sigma$ , then for any  $\Delta t > 0$ , the solution of the iteration (4.1)-(4.2) satisfies*

$$(U_K^{n,s}, V_K^{n,s}) \in \Sigma, \quad \forall K \in \mathcal{J}, \quad 0 \leq n \leq N, \quad s \geq 0. \quad (4.3)$$

---

**Algorithm 1** The IRP-preserving iteration
 

---

- 1: Compute the initial vector  $(U^0, V^0)$ ;
  - 2:  $n = 0$ ;
  - 3: **while**  $t^{n+1} \leq T$  **do**
  - 4:   Let  $s = 0$ ;
  - 5:   Take  $(U^{n+1,0}, V^{n+1,0}) = (U^n, V^n)$ ;
  - 6:   **while**  $\|U^{n+1,s+1} - U^{n+1,s}\|_\infty > \varepsilon_{non}$  or  $\|V^{n+1,s+1} - V^{n+1,s}\|_\infty > \varepsilon_{non}$  **do**
  - 7:     Solve the linear system (4.1)-(4.2);
  - 8:     Let  $s = s + 1$ ;
  - 9:   **end while**
  - 10:   Let  $n = n + 1$ ;
  - 11: **end while**
- 

*Proof.* The proof of this theorem is similar to that of Theorem 3.1. We assume that the reaction function is mixed quasimonotone, where  $f_1$  is quasimonotone nonincreasing and  $f_2$  is quasimonotone nondecreasing. The proofs for other types of quasimonotone reaction functions are similar. It is easy to see that  $(U_K^0, V_K^0) \in \Sigma$  for any  $K \in \mathcal{J}_{in} \cup \mathcal{J}_{out}$ . Suppose that (4.3) holds for any  $n \leq m+1$ ,  $s \leq s_0$ , where  $m \geq 0$ ,  $s_0 \geq 0$ . If (4.3) is proved for  $n = m+1$ ,  $s = s_0 + 1$ , then the theorem follows immediately.

Denote  $K_{\max,U}$ ,  $K_{\min,U}$ ,  $K_{\max,V}$ ,  $K_{\min,V}$  such that

$$\begin{aligned} U_{K_{\max,U}}^{m+1,s_0+1} &= \max_{K \in \mathcal{J}} U_K^{m+1,s_0+1}, & U_{K_{\min,U}}^{m+1,s_0+1} &= \min_{K \in \mathcal{J}} U_K^{m+1,s_0+1}, \\ V_{K_{\max,V}}^{m+1,s_0+1} &= \max_{K \in \mathcal{J}} V_K^{m+1,s_0+1}, & V_{K_{\min,V}}^{m+1,s_0+1} &= \min_{K \in \mathcal{J}} V_K^{m+1,s_0+1}. \end{aligned}$$

The proof can be divided into two steps. The first step is to prove that  $U_{K_{\max,U}}^{m+1,s_0+1} \leq M_1$ .

Let us suppose that  $U_{K_{\max,U}}^{m+1,s_0+1} > M_1$  holds. Starting from (4.1) and using a derivation similar to (3.20), it follows that

$$\begin{aligned} \frac{U_{K_{\max,U}}^{m+1,s_0+1} - M_1}{\Delta t} &\leq \frac{U_{K_{\max,U}}^{m+1,s_0+1} - U_{K_{\max,U}}^m}{\Delta t} \\ &\leq \lambda(U_{K_{\max,U}}^{m+1,s_0} - U_{K_{\max,U}}^{m+1,s_0+1}) + f_1(U_{K_{\max,U}}^{m+1,s_0}, V_{K_{\max,U}}^{m+1,s_0}). \end{aligned} \quad (4.4)$$

Since  $f_1$  is nonincreasing with respect to  $v$ , we have  $f_1(U_{K_{\max,U}}^{m+1,s_0}, V_{K_{\max,U}}^{m+1,s_0}) \leq f_1(U_{K_{\max,U}}^{m+1,s_0}, m_2)$ . Similar to the derivation of (3.21), it holds that

$$\begin{aligned} \frac{U_{K_{\max,U}}^{m+1,s_0+1} - M_1}{\Delta t} &\leq \lambda(U_{K_{\max,U}}^{m+1,s_0} - U_{K_{\max,U}}^{m+1,s_0+1}) + f_1(U_{K_{\max,U}}^{m+1,s_0}, m_2) - f_1(M_1, m_2) \\ &\leq \lambda(U_{K_{\max,U}}^{m+1,s_0} - M_1) + \lambda(M_1 - U_{K_{\max,U}}^{m+1,s_0}) = 0, \end{aligned} \quad (4.5)$$



which contradicts with  $U_{K_{\max,U}}^{m+1,s_0+1} > M_1$ . Hence we have  $U_{K_{\max,U}}^{m+1,s_0+1} \leq M_1$ .  $U_{K_{\min,U}}^{m+1,s_0+1} \geq m_1$  can be proved similarly. It means that  $U_K^{m+1,s_0+1} \in [m_1, M_1]$  for any  $K \in \mathcal{J}$ .

The second step is to show that  $V^{m+1,s_0+1} \in [m_2, M_2]$ .

If  $V^{m+1,s_0+1} \in [m_2, M_2]$  does not hold, then we have  $V_{K_{\max,V}}^{m+1,s_0+1} > M_2$  or  $V_{K_{\min,V}}^{m+1,s_0+1} < m_2$ .

Let us suppose that  $V_{K_{\max,V}}^{m+1,s_0+1} > M_2$  holds. Similar to (4.4), it follows that

$$\frac{V_{K_{\max,V}}^{m+1,s_0+1} - M_2}{\Delta t} \leq \lambda(V_{K_{\max,V}}^{m+1,s_0} - V_{K_{\max,V}}^{m+1,s_0+1}) + f_2(U_{K_{\max,V}}^{m+1,s_0+1}, V_{K_{\max,V}}^{m+1,s_0}). \quad (4.6)$$

According to the monotonicity of  $f_2$  with respect to  $u$ , we have  $f_2(U_{K_{\max,V}}^{m+1,s_0+1}, V_{K_{\max,V}}^{m+1,s_0}) \leq f_2(M_1, V_{K_{\max,V}}^{m+1,s_0})$ . Similar to the derivation of (4.5), it can be shown that

$$\frac{V_{K_{\max,V}}^{m+1,s_0+1} - M_2}{\Delta t} \leq 0,$$

which contradicts with  $V_{K_{\max,V}}^{m+1,s_0+1} > M_2$ . Hence we have  $V_{K_{\max,V}}^{m+1,s_0+1} \leq M_2$ . Similarly, we can prove that  $V_{K_{\min,V}}^{m+1,s_0+1} \geq m_2$ . It means that  $V_K^{m+1,s_0+1} \in [m_2, M_2]$  for any  $K \in \mathcal{J}$ . This completes the proof.  $\square$

## 5 Numerical experiments

In this section, numerical examples with different models are presented to show the accuracy and the IRP-preserving property of the finite volume scheme. The comparison results with the nine-point scheme are shown to demonstrate that the nine-point scheme fails to preserve the invariant regions, which indicates the advantage of the IRP-preserving scheme. In the numerical examples, we use

$$\begin{aligned} \varepsilon_u^2 &= \left[ \sum_{K \in \mathcal{J}_{in}} (U_K - u(K))^2 m(K) \right]^{1/2}, & \varepsilon_v^2 &= \left[ \sum_{K \in \mathcal{J}_{in}} (V_K - v(K))^2 m(K) \right]^{1/2}, \\ \varepsilon_u^F &= \left[ \sum_{K \in \mathcal{J}} (F_{K,\sigma} - \mathcal{F}_{K,\sigma})^2 \right]^{1/2}, & \varepsilon_v^F &= \left[ \sum_{K \in \mathcal{J}} (\tilde{F}_{K,\sigma} - \tilde{\mathcal{F}}_{K,\sigma})^2 \right]^{1/2} \end{aligned}$$

to evaluate approximate the  $L^2$  errors and the normal flux errors of  $u$  and  $v$ , respectively.

### 5.1 Example 1

In the first example, we consider the problem with continuous diffusion coefficients on  $\Omega = (0,1) \times (0,1)$ . The coefficients  $\kappa_1 = R_1 D_1 R_1^T$  and  $\kappa_2 = R_2 D_2 R_2^T$ , where  $R_1, R_2, D_1$  and  $D_2$

are given by

$$R_1 = \begin{pmatrix} \cos\theta_1 & -\sin\theta_1 \\ \sin\theta_1 & \cos\theta_1 \end{pmatrix}, \quad D_1 = \begin{pmatrix} k_1 & 0 \\ 0 & k_2 \end{pmatrix}$$

and

$$R_2 = \begin{pmatrix} \cos\theta_2 & -\sin\theta_2 \\ \sin\theta_2 & \cos\theta_2 \end{pmatrix}, \quad D_2 = \begin{pmatrix} k_3 & 0 \\ 0 & k_4 \end{pmatrix}.$$

We take  $\theta_1 = \frac{5\pi}{12}$ ,  $\theta_2 = \frac{\pi}{3}$ ,  $k_1 = 1 + 2x^2 + y^2$ ,  $k_2 = 1 + x^2 + 2y^2$ ,  $k_3 = 1 + x^2 + 2y^2$ ,  $k_4 = 1 + 2x^2 + y^2$ . We set  $f_1(u, v) = u(1-u)(u-0.1)$  and  $f_2(u, v) = u - v$  and take the exact solution

$$\begin{aligned} u(x, y, t) &= e^{-t} \sin(\pi x) \sin(\pi y), \\ v(x, y, t) &= e^{-t} \cos(\pi x) \cos(\pi y). \end{aligned}$$

The exact solution provides the Dirichlet boundary conditions. We add linear source terms in the right sides of the model (2.1)-(2.2), which can be calculated from the exact solution correspondingly.

We set the final time  $T = 1$  and a sufficiently small time step  $\Delta t = 1E-4$ . This example only tests the spacial convergence order, and no investigation on IRP was conducted. Denote by  $N_c$  the number of cells. We display the  $L^2$  errors and flux errors on the random quadrilateral and triangular meshes in Tables 2-3, respectively. The two types of random meshes are presented in Figs 2-3. From these tables, we observe that the  $L^2$  errors obtain second-order convergence rate on both the random quadrilateral and triangular meshes, and the flux errors obtain first-order convergence rate on the random quadrilateral meshes and obtain higher than first-order convergence rate on random triangular meshes.

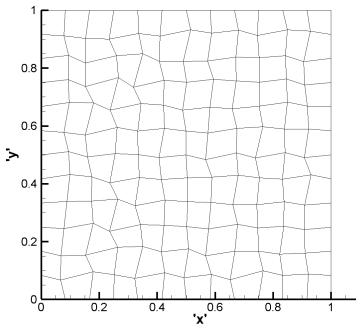


Figure 2: The random quadrilateral meshes.

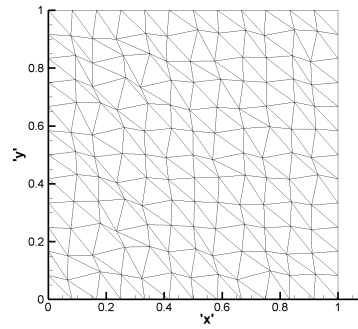


Figure 3: The random triangular meshes.

Table 2: The errors for Example 1 on the random quadrilateral meshes.

$N_c$	144	576	2304	9216
$\varepsilon_u^2$	1.21E-03	3.98E-04	1.04E-04	2.21E-05
order		1.61	1.93	2.23
$\varepsilon_u^F$	1.80E-02	8.27E-03	3.90E-03	2.02E-03
order		1.12	1.08	0.94
$\varepsilon_v^2$	1.60E-03	4.14E-04	1.05E-04	2.63E-05
order		1.94	1.98	1.99
$\varepsilon_v^F$	1.95E-02	8.50E-03	4.00E-03	1.96E-03
order		1.19	1.08	1.02

Table 3: The errors for Example 1 on the random triangular meshes.

$N_c$	288	1152	4608	18432
$\varepsilon_u^2$	9.32E-04	2.45E-04	5.96E-05	1.38E-05
order		1.92	2.03	2.10
$\varepsilon_u^F$	1.98E-02	6.23E-03	2.16E-03	9.31E-04
order		1.66	1.52	1.21
$\varepsilon_v^2$	8.97E-04	2.52E-04	6.31E-05	1.56E-05
order		1.83	1.99	2.01
$\varepsilon_v^F$	1.87E-02	6.65E-03	2.69E-03	1.11E-03
order		1.49	1.30	1.27

## 5.2 Example 2

In this example, we test the accuracy of our scheme under the problem with discontinuous diffusion coefficient on  $\Omega = (0,1) \times (0,1)$ . We consider the exact solution

$$u(x,y,t) = \begin{cases} e^{-t} (x - \frac{2}{3}) (x^3 + y^3), & \text{if } x \leq \frac{2}{3}, \\ 4e^{-t} (x - \frac{2}{3}) (x^3 + y^3), & \text{if } x > \frac{2}{3}, \end{cases}$$

$$v(x,y,t) = \begin{cases} e^{-t} (x - \frac{2}{3}) (x^2 - y^2), & \text{if } x \leq \frac{2}{3}, \\ 4e^{-t} (x - \frac{2}{3}) (x^2 - y^2), & \text{if } x > \frac{2}{3}, \end{cases}$$

and take the diffusion coefficient

$$\kappa_1 = \kappa_2 = \begin{cases} 4I, & \text{if } x \leq \frac{2}{3}, \\ I, & \text{if } x > \frac{2}{3}. \end{cases}$$

The functions  $f_1(u,v)$  and  $f_2(u,v)$  are

$$f_1(u,v) = u^2 - e^v,$$

$$f_2(u,v) = u^3 - v,$$

and the linear source functions are calculated correspondingly.

We set the final time  $T = 1$  and a sufficiently small time step  $\Delta t = 1E-4$  in order to test the spacial accuracy, no investigation on IRP was conducted. Tables 4-5 provide the  $L^2$  norm of errors in solutions and fluxes on two types of random meshes. The numerical results reveal that our scheme obtains second-order convergence rate for the  $L^2$  errors of solutions and is higher than first-order convergence rate for the flux errors.

Table 4: The errors for Example 2 on the random quadrilateral meshes.

$N_c$	144	576	2304	9216
$\varepsilon_u^2$	3.44E-03	8.96E-04	2.26E-04	5.67E-05
order		1.94	1.98	1.99
$\varepsilon_u^F$	2.14E-02	7.63E-03	3.03E-03	1.43E-03
order		1.48	1.33	1.08
$\varepsilon_v^2$	2.26E-03	5.77E-04	1.45E-04	3.66E-05
order		1.96	1.99	1.98
$\varepsilon_v^F$	1.62E-02	5.84E-03	2.38E-03	1.11E-03
order		1.47	1.29	1.10

Table 5: The errors for Example 2 on the random triangular meshes.

$N_c$	288	1152	4608	18432
$\varepsilon_u^2$	2.02E-03	5.44E-04	1.36E-04	3.42E-05
order		1.89	1.99	1.99
$\varepsilon_u^F$	1.41E-02	4.61E-03	1.53E-03	6.10E-04
order		1.61	1.59	1.32
$\varepsilon_v^2$	7.40E-04	2.00E-04	4.94E-05	1.27E-05
order		1.88	2.01	1.95
$\varepsilon_v^F$	1.00E-02	3.24E-03	1.09E-03	4.00E-04
order		1.62	1.56	1.45

### 5.3 Example 3

In Example 3, we consider a semilinear parabolic system illustrating the superconductivity of liquids, where  $\kappa_1$  and  $\kappa_2$  are positive definite diagonal matrices, and the nonlinear reaction-diffusion terms are as follows:

$$\begin{aligned} f_1(u,v) &= (1-u^2-v^2)u, \\ f_2(u,v) &= (1-u^2-v^2)v. \end{aligned}$$

$(f_1, f_2)$  is quasimonotone nonincreasing in  $[0, +\infty) \times [0, +\infty)$ . The domain of this example is set to be a square with a hole  $\Omega = (0,1)^2 \setminus [4/9, 5/9]^2$ , where internal and external

boundaries are denoted by  $\Gamma_1$  and  $\Gamma_2$ , respectively. Let the diffusion coefficients  $\kappa_1$  and  $\kappa_2$  be discontinuous at  $\Gamma$ , where  $\Gamma$  are composed of the edges of the square  $(2/9, 7/9)^2$ . The domain  $\Omega$  is divided into two parts by  $\Gamma$ , where  $\Omega_1 = (0,1)^2 \setminus [2/9, 7/9]^2$  and  $\Omega_2 = \Omega \setminus \Omega_1$ . We take the diffusion coefficients

$$\kappa_1 = \begin{cases} 2I, & \text{in } \Omega_1, \\ \begin{pmatrix} y^2 + \varepsilon & -(1-\varepsilon)xy \\ -(1-\varepsilon)xy & x^2 + \varepsilon \end{pmatrix}, & \text{in } \Omega_2, \end{cases}$$

$$\kappa_2 = \begin{cases} I, & \text{in } \Omega_1, \\ \begin{pmatrix} y^2 + \varepsilon & (1-\varepsilon)xy \\ (1-\varepsilon)xy & x^2 + \varepsilon \end{pmatrix}, & \text{in } \Omega_2, \end{cases}$$

where  $\varepsilon = 5E-3$ , and take the initial and boundary conditions as

$$g_1(x, y, t) = \begin{cases} 0, & \text{in } \Gamma_1, \\ 1, & \text{in } \Gamma_2, \end{cases} \quad g_2(x, y, t) = \begin{cases} 1, & \text{in } \Gamma_1, \\ 0, & \text{in } \Gamma_2, \end{cases}$$

and

$$u_0(x, y) = \begin{cases} 0, & \text{in } \Omega_1, \\ 1, & \text{in } \Omega_2, \end{cases} \quad v_0(x, y) = \begin{cases} 1, & \text{in } \Omega_1, \\ 0, & \text{in } \Omega_2. \end{cases}$$

It is obvious that  $[0,1] \times [0,1]$  is its invariant region, and the Lipschitz constant  $\lambda = 5$ .

We observe the invariant region properties on random quadrilateral meshes with  $N_c = 2916$  and random triangular meshes with  $N_c = 5832$ , respectively. The numerical solutions are displayed in Figs 4-5 for random quadrilateral meshes, and in Figs 6-7 for random triangular meshes, respectively. The minimum and maximum values for  $U$  on random quadrilateral are 0 and 1, respectively. Similarly, the minimum and maximum values for  $V$  on random triangular meshes are 0 and 1. The numerical results demonstrate the IRPs of our scheme.

#### 5.4 Example 4

In Example 4, we consider a simplified model of the Belousov-Zhabotinski reaction on  $\Omega = (0,1) \times (0,1)$ , which is a classical model in non-equilibrium thermodynamics. This model takes the reaction functions

$$\begin{aligned} f_1(u, v) &= u(a - bu - cv), \\ f_2(u, v) &= -uv, \end{aligned}$$

where  $a, b, c$  are positive constants. When  $u \geq 0$  and  $v \geq 0$ , the  $(f_1, f_2)$  are quasimonotone nonincreasing, and  $f_1$  and  $f_2$  are Lipschitz continuous in any finite region of  $(u, v)$ . We

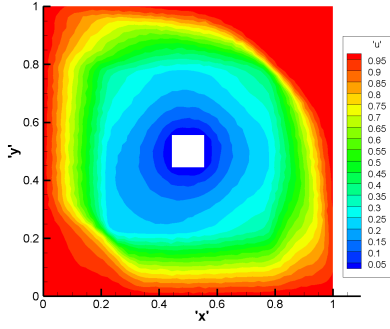


Figure 4: The numerical solution  $U$  of the IRP-preserving scheme for Example 3 on the random quadrilateral meshes ( $U_{\min}=0$ ,  $U_{\max}=1$ ).

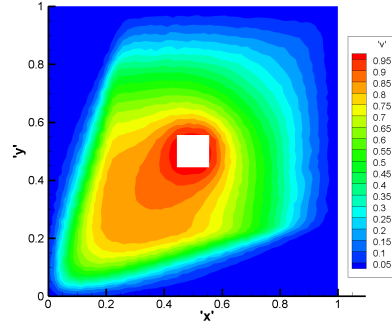


Figure 5: The numerical solution  $V$  of the IRP-preserving scheme for Example 3 on the random quadrilateral meshes ( $V_{\min}=1$ ,  $V_{\max}=1$ ).

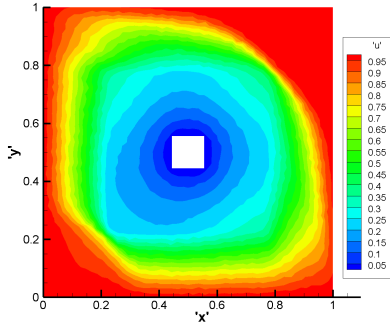


Figure 6: The numerical solution  $U$  of the IRP-preserving scheme for Example 3 on the random triangular meshes ( $U_{\min}=0$ ,  $U_{\max}=1$ ).

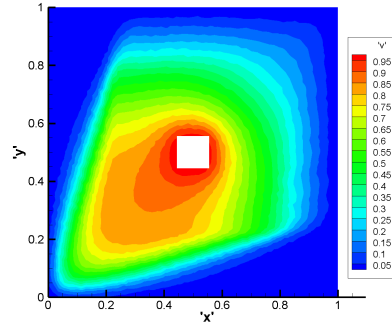


Figure 7: The numerical solution  $V$  of the IRP-preserving scheme for Example 3 on the random triangular meshes ( $V_{\min}=0$ ,  $V_{\max}=1$ ).

take  $a=1$ ,  $b=2$ ,  $c=10$  and take the functions

$$u_0(x,y) = g_1(x,y,t) = \begin{cases} 0, & \text{if } 2x - y \leq -\frac{1}{16}, \\ 8(2x - y) + 0.5, & \text{if } -\frac{1}{16} < 2x - y \leq \frac{1}{16}, \\ 1, & \text{if } 2x - y > \frac{1}{16}, \end{cases}$$

and

$$v_0(x,y) = g_2(x,y,t) = \begin{cases} 0, & \text{if } x + 2y \leq \frac{15}{16}, \\ 16(x + 2y) - 15, & \text{if } \frac{15}{16} < x + 2y \leq \frac{17}{16}, \\ 2, & \text{if } x + 2y > \frac{17}{16}. \end{cases}$$

A simple calculation gives  $(u_0, v_0), (g_1, g_2) \in [0,1] \times [0,2]$ , the Lipschitz constant  $\lambda = 35$ . According to Lemma 2.1, the invariant region of the exact solution is  $[0,1] \times [0,2]$ .

We take  $T = 1$  and  $\Delta t = 1\text{E-}3$ . We solve the problem using our scheme and the nine-point (N-P) scheme on the random quadrilateral meshes with  $N_c = 3600$  and random triangular meshes with  $N_c = 7200$ , respectively. The numerical solutions are presented in Figures 8-15. We denote the maximum and minimum of the solution vector  $U$  as  $U_{\max}$  and  $U_{\min}$ , respectively.  $V_{\max}$  and  $V_{\min}$  are denoted similarly. The numbers of overshoots and undershoots of numerical solution are denoted as  $N_c^o$  and  $N_c^u$ , and the corresponding percentages are indicated by “pct”. Table 6 and Table 7 summarize the maxima and minima, the numbers of overshoots and undershoots and their percentages of the two schemes, respectively. As shown in Tables 6-7, the solution of our scheme on both meshes remains within the range of  $[0,1] \times [0,2]$ , whereas the nine-point scheme fails to preserve the IRP. In the latter case, we set the numerical solutions that fall outside the invariant region to gray for visual clarity.

Table 6: The maxima and minima of the IRP-preserving scheme and nine-point scheme for Example 4 on random quadrilateral meshes.

method	$U_{\max}$	$N_c^o$	pct	$U_{\min}$	$N_c^u$	pct
IRP	0	0	0.00%	1	0	0.00%
NP	1.0290	562	15.61%	-2.1341E-02	419	11.64%
	$V_{\max}$	$N_c^o$	pct	$V_{\min}$	$N_c^u$	pct
IRP	0	0	0.00%	2	0	0.00%
NP	2.0641	655	18.19%	-4.2454E-02	418	11.61%

Table 7: The maxima and minima of the IRP-preserving scheme and nine-point scheme for Example 4 on random triangular meshes.

method	$U_{\max}$	$N_c^o$	pct	$U_{\min}$	$N_c^u$	pct
IRP	0	0	0.00%	1	0	0.00%
NP	1.0186	699	9.71%	-1.7108E-02	777	10.79%
	$V_{\max}$	$N_c^o$	pct	$V_{\min}$	$N_c^u$	pct
IRP	0	0	0.00%	2	0	0.00%
NP	2.0694	1535	21.32%	-4.1207E-02	821	11.40%

## 6 Conclusion

A finite volume method preserving the invariant region property is constructed for coupled quasimonotone reaction-diffusion systems on general polygonal meshes. The backward Euler method and DMP-preserving finite volume scheme in [16] are employed to approximate the time derivatives and the diffusion terms, respectively, which yields a nonlinear and conservative scheme. The iterative scheme is constructed to solve the nonlinear system. We prove that both the nonlinear scheme and the iterative method

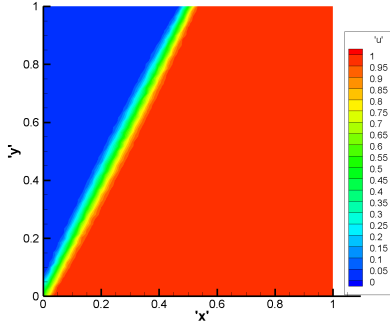


Figure 8: The numerical solution  $U$  of the IRP-preserving scheme for Example 4 on the random quadrilateral meshes ( $U_{\min}=0$ ,  $U_{\max}=1$ ).

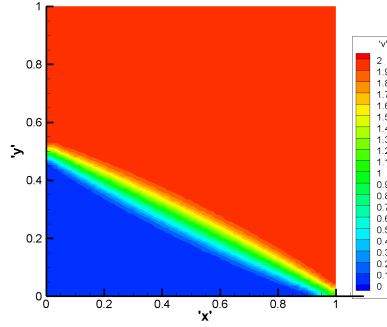


Figure 9: The numerical solution  $V$  of the IRP-preserving scheme for Example 4 on the random quadrilateral meshes ( $V_{\min}=0$ ,  $V_{\max}=2$ ).

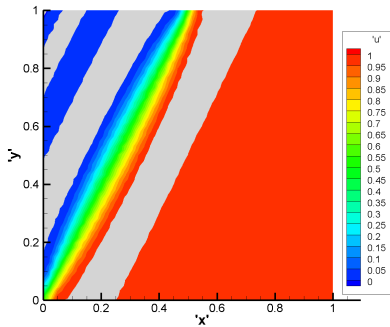


Figure 10: The numerical solution  $U$  of the nine-point scheme for Example 4 on the random quadrilateral meshes ( $U_{\min}=-2.1341\text{E-}2$ ,  $U_{\max}=1.0290$ ).

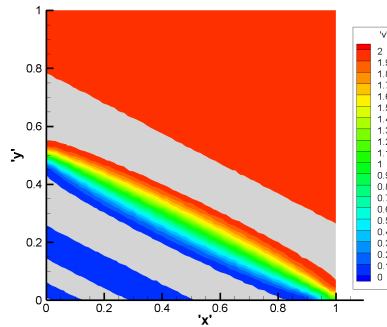


Figure 11: The numerical solution  $V$  of the nine-point scheme for Example 4 on the random quadrilateral meshes ( $V_{\min}=-4.2454\text{E-}2$ ,  $V_{\max}=2.0641$ ).

preserve the IRP for three kinds of quasimonotone systems. Finally, some numerical examples are given to illustrate the accuracy and the IRP-preserving property.

## Acknowledgments

This work is partially supported by the National Natural Science Foundation of China (12201246), LCP Fund for Young Scholar (6142A05QN22010), National Key R&D Program of China (2020YFA0713601), and by the Key Laboratory of Symbolic Computation and Knowledge Engineering of Ministry of Education, Jilin University, Changchun, 130012, P.R. China.



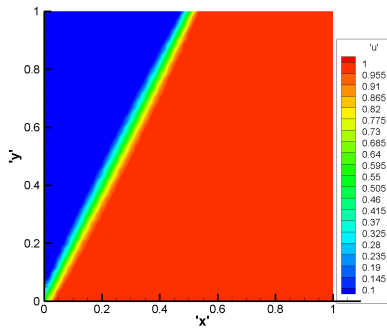


Figure 12: The numerical solution  $U$  of the IRP-preserving scheme for Example 4 on the random triangular meshes ( $U_{\min}=0$ ,  $U_{\max}=1$ ).

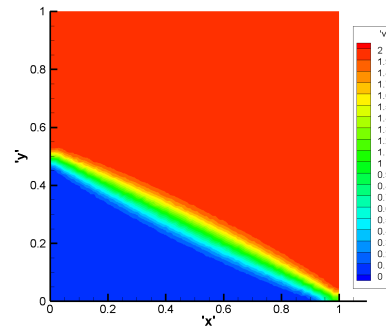


Figure 13: The numerical solution  $V$  of the IRP-preserving scheme for Example 4 on the random triangular meshes ( $V_{\min}=0$ ,  $V_{\max}=2$ ).

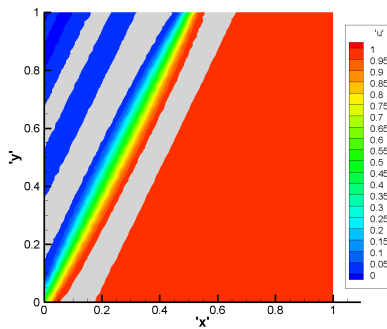


Figure 14: The numerical solution  $U$  of the nine-point scheme for Example 4 on the random triangular meshes ( $U_{\min}=1.7108E-2$ ,  $U_{\max}=1.0186$ ).

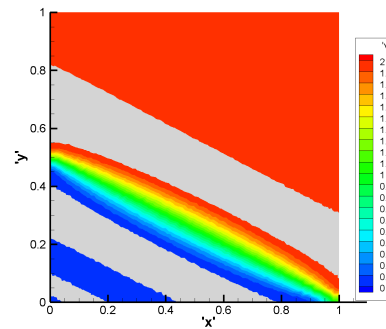


Figure 15: The numerical solution  $V$  of the nine-point scheme for Example 4 on the random triangular meshes ( $V_{\min}=-4.1207E-2$ ,  $V_{\max}=2.0694$ ).

## References

- [1] Y. Bourgault, Y. Coudière, and C. Pierre, Existence and uniqueness of the solution for the bidomain model used in cardiac electrophysiology, *Nonlinear Analysis: Real World Applications*, 10 (2009-02), pp. 458–482.
- [2] P. Colli-Franzone, L. Guerri, and B. Taccardi, Modeling ventricular excitation: Axial and orthotropic anisotropy effects on wavefronts and potentials, *Mathematical Biosciences*, 188 (2004-03), pp. 191–205.
- [3] D. Conte, G. Pagano, and B. Paternoster, Nonstandard finite differences numerical methods for a vegetation reaction–diffusion model, *Journal of Computational and Applied Mathematics*, 419 (2023-02), p. 114790.
- [4] Q. Du, M. D. Gunzburger, and J. S. Peterson, Analysis and approximation of the Ginzburg-Landau model of superconductivity, *SIAM Review*, 34 (1992), pp. 54–81.
- [5] Q. Du, L. Ju, X. Li, and Z. Qiao, Maximum bound principles for a class of semilinear parabolic equations and exponential time-differencing schemes, *SIAM Review*, 63 (2021), pp. 317–359.

- [6] P. C. Fife, *Mathematical aspects of reacting and diffusing systems*, Springer-Verlag, 1979.
- [7] M. Frittelli, A. Madzvamuse, I. Sgura, and C. Venkataraman, Numerical preservation of velocity induced invariant regions for reaction–diffusion systems on evolving surfaces, *Journal of Scientific Computing*, 77 (2018-11), pp. 971–1000.
- [8] Y. Gong, B. Ji, and H. Liao, A maximum bound principle preserving iteration technique for a class of semilinear parabolic equations, *Applied Numerical Mathematics*, 184 (2023-02), pp. 482–495.
- [9] U. Hornung and W. Jäger, Diffusion, convection, adsorption, and reaction of chemicals in porous media, *Journal of Differential Equations*, 92 (1991-08), pp. 199–225.
- [10] M. Hunacek, *Representations of finite groups of Lie type (2nd edn.)*, Cambridge University Press (2020), *Mathematical Gazette*, 106, pp. 372–373.
- [11] J. W. Jerome, Fully discrete stability and invariant rectangular regions for reaction-diffusion systems, *SIAM Journal on Numerical Analysis*, 21 (1984-12), pp. 1054–1065.
- [12] M. Justin, G. Betchewe, S. Y. Doka, and K. T. Crepin, Exact solutions of a semiconductor nonlinear reaction diffusion equation through factorization method, *Applied Mathematics and Computation*, 219 (2012-11), pp. 2917–2922.
- [13] X. Li, L. Ju, and T.-T.-P. Hoang, Overlapping domain decomposition based exponential time differencing methods for semilinear parabolic equations, *Bit Numerical Mathematics*, 61 (2021-03), pp. 1–36.
- [14] J. Sembera and M. Benes, Nonlinear Galerkin method for reaction–diffusion systems admitting invariant regions, *Journal of Computational and Applied Mathematics*, (2001), pp. 163–176.
- [15] Z. Sheng and G. Yuan, A nine point scheme for the approximation of diffusion operators on distorted quadrilateral meshes, *SIAM Journal on Scientific Computing*, 30 (2008), pp. 1341–1361.
- [16] Z. Sheng and G. Yuan, A nonlinear scheme preserving maximum principle for heterogeneous anisotropic diffusion equation, *Journal of Computational and Applied Mathematics*, 436 (2024-01), p. 115438.
- [17] J. Smoller, *Shock waves and reaction-diffusion equations*, Springer, 2 ed., 1999.
- [18] R. Spigler and D. H. Zanette, Reaction-diffusion models from the Fokker-Planck formulation of chemical processes, *IMA Journal on Applied Mathematics*, 49 (1992), pp. 217–229.
- [19] H. Zhou, Z. Sheng, and G. Yuan, A finite volume scheme preserving the invariant region property for the coupled system of FitzHugh-Nagumo equations on distorted meshes, *Computers & Mathematics with Applications*, 117 (2022-07), pp. 39–52.